

1 **Reassessing the ratio of glyoxal to formaldehyde as an**  
2 **indicator of hydrocarbon precursor speciation**

3  
4 **J. Kaiser<sup>1</sup>, G. M. Wolfe<sup>2,3</sup>, K. E. Min<sup>4,5,\*</sup>, S. S. Brown<sup>5,6</sup>, C. C. Miller<sup>7</sup>, D. J. Jacob<sup>7,8</sup>, J.**  
5 **A. deGouw<sup>4,5</sup>, M. Graus<sup>4,5</sup>, T. F. Hanisco<sup>3</sup>, J. Holloway<sup>4,5</sup>, J. Peischl<sup>4,5</sup>, I. B.**  
6 **Pollack<sup>4,5</sup>, T. B. Ryerson<sup>5</sup>, C. Warneke<sup>4,5</sup>, R. A. Washenfelder<sup>4,5</sup>, and F. N.**  
7 **Keutsch<sup>1,\*\*</sup>**

8 <sup>1</sup>Department of Chemistry, University of Wisconsin-Madison, Madison, WI, USA

9 <sup>2</sup>Joint Center for Earth Systems Technology, University of Maryland Baltimore County,  
10 Baltimore, Maryland, USA

11 <sup>3</sup>Atmospheric Chemistry and Dynamics Laboratory, NASA Goddard Space Flight Center,  
12 Greenbelt, Maryland, USA

13 <sup>4</sup>Cooperative Institute for Research in Environmental Sciences, University of Colorado Boulder,  
14 Boulder, Colorado, USA

15 <sup>5</sup>Chemical Sciences Division, NOAA Earth System Research Laboratory, Boulder, Colorado,  
16 USA

17 <sup>6</sup>Department of Chemistry and Biochemistry, University of Colorado, Boulder, Colorado, USA

18 <sup>7</sup>Department of Earth and Planetary Sciences, Harvard University, Cambridge, Massachusetts,  
19 USA

20 <sup>8</sup>School of Engineering and Applied Sciences, Harvard University, Cambridge, Massachusetts,  
21 USA

22 \*now at School of Environmental Science and Engineering, Gwangju Institute for Science and  
23 Technology, Gwangju, Korea

24 \*\*now at School of Engineering and Applied Sciences and Department of Chemistry and  
25 Chemical Biology, Harvard University, Cambridge, Massachusetts, USA

1 Correspondence to: J. Kaiser (jen.b.kaiser@gmail.com)

1    **Abstract**

2    The yield of formaldehyde (HCHO) and glyoxal (CHOCHO) from oxidation of volatile organic  
3    compounds (VOCs) depends on precursor VOC structure and the concentration of NO<sub>x</sub> (NO<sub>x</sub> =  
4    NO + NO<sub>2</sub>). Previous work has proposed that the ratio of CHOCHO to HCHO (R<sub>GF</sub>) can be used  
5    as an indicator of precursor VOC speciation, and absolute concentrations of the CHOCHO and  
6    HCHO as indicators of NO<sub>x</sub>. Because this metric is measurable by satellite, it is potentially  
7    useful on a global scale; however, absolute values and trends in R<sub>GF</sub> have differed between  
8    satellite and ground-based observations. To investigate potential causes of previous  
9    discrepancies and the usefulness of this ratio, we present measurements of CHOCHO and HCHO  
10   over the Southeast United States (SE US) from the 2013 SENEX flight campaign, and compare  
11   these measurements with OMI satellite retrievals. High time-resolution flight measurements  
12   show that high R<sub>GF</sub> is associated with monoterpene emissions, low R<sub>GF</sub> is associated with  
13   isoprene oxidation, and emissions associated with oil and gas production can lead to small-scale  
14   variation in regional R<sub>GF</sub>. During the summertime in the SE US, R<sub>GF</sub> is not a reliable diagnostic  
15   of anthropogenic VOC emissions, as HCHO and CHOCHO production are dominated by  
16   isoprene oxidation. Our results show that the new CHOCHO retrieval algorithm reduces the  
17   previous disagreement between satellite and in situ R<sub>GF</sub> observations. As the absolute values and  
18   trends in R<sub>GF</sub> observed during SENEX are largely reproduced by OMI observations, we conclude  
19   that satellite-based observations of R<sub>GF</sub> can be used alongside knowledge of land-use as a global  
20   diagnostic of dominant hydrocarbon speciation.

21

22    **1    Introduction**

23    Though volatile organic compounds (VOCs) are present only in trace amounts in the atmosphere,  
24    their presence can drive the formation of pollutants such as secondary organic aerosol and ozone.  
25    The impact of VOC emissions on tropospheric chemistry depends on the speciation of emitted  
26    VOCs and their degradation pathways. As many as 10<sup>5</sup> different species of VOCs are estimated  
27    to have been measured in the atmosphere (Goldstein and Galbally, 2007). While an air mass will  
28    usually contain a large variety of VOCs, often a particular species or subset of species (e.g.  
29    biogenics) will dominate the photochemistry, giving rise to the production of a range of

1 oxygenated VOCs (OVOCs). Thus, OVOCs can provide downstream constraints on the rates and  
2 pathways of VOC oxidation.

3 Here, we focus on the production of two ubiquitous OVOCs: formaldehyde (HCHO) and glyoxal  
4 (CHOCHO). HCHO is formed from the oxidation of nearly every anthropogenic and biogenic  
5 VOC (AVOC/BVOC, respectively). Though photochemical formation is thought to dominate the  
6 HCHO global budget (Fortems-Cheiney et al., 2012), direct HCHO emissions from pyrogenic,  
7 anthropogenic, and biogenic activity have also been observed (Guenther et al., 1995;  
8 Kesselmeier et al., 1997; Holzinger et al., 1999; Garcia et al., 2006; DiGangi et al., 2011).  
9 CHOCHO is formed from the oxidation of a smaller subset of VOCs, particularly alkenes,  
10 aromatics, isoprene, and monoterpenes (Fu et al., 2008). Direct emission from biofuel and  
11 biomass burning can also be a significant source of CHOCHO (McDonald et al., 2000; Hays et  
12 al., 2002; Christian et al., 2003; Greenberg et al., 2006). Because the yields of HCHO and  
13 CHOCHO differ between classes of VOC, and because their atmospheric lifetimes are similar,  
14 the relative abundance of CHOCHO and HCHO has been hypothesized to reflect the speciation  
15 of VOCs contributing to total VOC reactivity (Vrekoussis et al., 2010; DiGangi et al., 2012;  
16 MacDonald et al., 2012; Li et al., 2014; Miller et al., 2014).

17 A major motivating factor for examining the ratio of glyoxal to formaldehyde ( $R_{GF}$ , in units of  
18 mole/mole) is the ability to quantify both compounds on a global scale from satellite retrievals.  
19 Currently, HCHO and CHOCHO are the only two OVOCs with UV-Visible absorption features  
20 strong enough to enable solar backscatter measurements of vertical column densities. Long term  
21 continuous HCHO columns are available from four satellite-based instruments: GOME (Global  
22 Ozone Monitoring Experiment), SCIAMACHY (SCanning Imaging Absorption spectroMeter for  
23 Atmospheric CHartographY), OMI (Ozone Monitoring Instrument), and GOME-2. CHOCHO  
24 retrievals are available from SCIAMACHY, OMI, and GOME-2. Satellite-derived  $R_{GF}$  could be  
25 a promising diagnostic tool in determining the speciation of VOC precursors that lead to  
26 pollution formation in a given region, especially as retrievals improve in temporal and spatial  
27 resolution.

28 Table 1 summarizes previously published observations and conclusions about  $R_{GF}$ . Using  
29 GOME-2 satellite retrievals, Vrekoussis et al. (2010) observed  $R_{GF}$  as low as 3% in

1 anthropogenic regions and between 4 and 6% over heavily vegetated regions. This was  
2 interpreted as an indication that anthropogenic precursors favor HCHO production relative to  
3 CHOCHO, while biogenic precursors favor CHOCHO production relative to HCHO. Primary  
4 emissions of HCHO were also thought to lower the observed  $R_{GF}$  in anthropogenic regions. In  
5 contrast, using ground-based measurements, DiGangi et al. (2012) observed  $R_{GF}$  values typically  
6 <2% in rural areas, while fresh anthropogenic influence increased  $R_{GF}$  to 4%. These observations  
7 yielded a directly contradictory interpretation: AVOCs favor CHOCHO production, whereas  
8 BVOCs favor HCHO production. Furthermore, DiGangi et al. (2012) showed that, given the  
9 same VOC speciation,  $R_{GF}$  was invariant despite changes in observed NO<sub>x</sub> concentrations. They  
10 proposed that this was a result of CHOCHO and HCHO formation primarily via the high-NO<sub>x</sub>  
11 pathway of organic peroxy radical (RO<sub>2</sub>) reactions, which in turn makes the absolute  
12 concentration of either OVOC equally dependant on NO<sub>x</sub> and therefore leaves  $R_{GF}$  unchanged.

13 Following these two investigations, high values of  $R_{GF}$  (20-40%) were observed above an Asian  
14 tropical forest (MacDonald et al., 2012), agreeing qualitatively with the conclusion of Vrekoussis  
15 et al. that high  $R_{GF}$  is consistent with biogenic source areas. The reported  $R_{GF}$  values, however,  
16 are an order of magnitude greater than satellite observations (Vrekoussis et al., 2010; Miller et  
17 al., 2014). Li et al. (2014) report an average  $R_{GF}$  of 6% at a semi-rural site in Southern China.  
18 Both observations and model simulations showed that increasing AVOC emissions lead to an  
19 increase in  $R_{GF}$ . The model simulations indicated  $R_{GF}$  was controlled not only by VOC  
20 speciation, but also by NO<sub>x</sub> and OH mixing ratios, as well as physical processes such as  
21 CHOCHO deposition and aerosol uptake (Li et al., 2014). Recently, a new algorithm for the  
22 retrieval of CHOCHO from OMI was developed which lessens sensitivity to water vapor  
23 abundance and produces on-average lower CHOCHO vertical column densities due to the choice  
24 of reference sector (Miller et al., 2014). In contrast to the ranges of  $R_{GF}$  reported by Vrekoussis  
25 et al. (2010), the OMI retrieval yields high  $R_{GF}$  in areas associated with monoterpene emissions,  
26 intermediate  $R_{GF}$  in areas dominated by anthropogenic emissions, and low  $R_{GF}$  in regions  
27 associated with strong isoprene emissions.

28 The cause of the discrepancies between satellite and ground-based  $R_{GF}$  trends and absolute  
29 values are unknown. DiGangi et al. (2012) suggested column-integrated and ground-based  
30 measurements in forests may differ due to direct HCHO emissions, or boundary layer ratios

1 could be systematically lower than free troposphere ratios. Additionally, Miller et al. (2014)  
2 highlight interferences from water vapor, reference sector selection, and multi-year averaging as  
3 potential causes for the previous errors in satellite retrievals. Despite the different ranges and  
4 trends of observed values, all previously published work concludes that  $R_{GF}$  reflects at least in  
5 part the speciation of VOCs in a given air mass. If  $R_{GF}$  is to be used as a global tracer of VOC  
6 composition, all factors influencing  $R_{GF}$  must be fully elucidated, and satellite retrievals must be  
7 validated against field observations.

8 With flights transecting both anthropogenic and biogenic regions, as well as profiles extending  
9 from the boundary layer into the free troposphere, the 2013 SENEX (Southeast Nexus) field  
10 campaign provides an unprecedented opportunity to address these uncertainties. Unlike ground-  
11 based field campaigns, the flight campaign provides information about the vertical structure of  
12 the trace gasses and a direct, real-time comparison of  $R_{GF}$  in urban outflow and in the  
13 surrounding rural areas. To our knowledge, this data represents the first high-time resolution  
14 simultaneous in situ flight-based measurements of HCHO and CHOCHO. We present absolute  
15 mixing ratios of HCHO and CHOCHO observed during daytime flights in the Southeast United  
16 States (SE US) and discuss the observed relationships of  $R_{GF}$  with observed VOC precursors and  
17 anthropogenic influence. Finally, to investigate the applicability of our findings for global  
18 studies, we compare flight-based  $R_{GF}$  with those derived from OMI observations.

19

## 20 **2 Experimental Methods**

### 21 **2.1 SENEX flight measurements**

22 During the SENEX project in June and July of 2013, HCHO, CHOCHO, NO<sub>x</sub>, and VOC  
23 measurements were acquired simultaneously from the NOAA WP-3D research aircraft during 13  
24 daytime flights. An in-depth description of the SENEX science goals, NOAA WP-3D aircraft, all  
25 onboard instrumentation, and each flight plan can be found elsewhere (C. Warneke, in  
26 preparation, 2015). A summary of average conditions for each flight is provided in Table S1.

27 HCHO was measured at 1 Hz by the NASA In Situ Atmospheric Formaldehyde (ISAF)  
28 instrument (Cazorla et al., 2014), which is based on the FIber-Laser-Induced-Fluorescence

1 (FILIF) technique (Hottle et al., 2009; DiGangi et al., 2011; Kaiser et al., 2014). The reported  
2 accuracy of the HCHO measurements is 10%. CHOCHO was measured at 0.2 Hz by Airborne  
3 Cavity Enhanced Spectrometer (ACES) with 6% accuracy. (Washenfelder et al., 2011; K. Min,  
4 in preparation, 2015). The precision of the CHOCHO measurement was a significant fraction of  
5 the typical ambient concentration (32 ppt precision, with a typical concentration of 100-150  
6 pptv), such that precision is a more stringent limitation on data quality than accuracy relative to  
7 HCHO, for which the signal was consistently much larger (HCHO precision 25 ppt, with  
8 concentrations typically > 3 ppb).

9 NO and NO<sub>2</sub> were measured by ozone-induced chemiluminescence (CL) and UV photolysis  
10 followed by CL, respectively (Ryerson et al., 1998; Pollack et al., 2012). VOCs were measured  
11 at 20% accuracy using proton-transfer reaction mass spectrometry (de Gouw and Warneke,  
12 2007). Unless otherwise specified, all data shown here are filtered to remove in-cloud  
13 measurements, measurements below 200 m or above 1200 m, and data that may be affected by  
14 the exhaust of the WP-3D aircraft. R<sub>GF</sub> is calculated by averaging the 1 s HCHO data to the 5 s  
15 CHOCHO observations.

## 16 **2.2 Satellite retrievals**

17 The Ozone Monitoring Instrument (OMI) is a nadir viewing UV-Visible grating spectrometer,  
18 launched onboard the NASA Aura satellite in July 2004 (Levelt et al., 2006). OMI provides daily  
19 global coverage at high spatial resolution (13 x 24 km footprint at nadir). We use slant column  
20 densities ( $\Omega_s$ ) of HCHO and CHOCHO from 2006 to 2007 derived from fits to OMI spectra  
21 (González Abad et al., 2014; Miller et al., 2014). HCHO and CHOCHO are retrieved between  
22 328.5-365.5 nm and 435-461 nm respectively. Slant columns are adjusted to vertical column  
23 densities ( $\Omega_v$ ) using scattering weights ( $S(z)$ ) archived from the retrieval product, and species  
24 concentration profiles ( $n(z)$ ) from the GEOS-Chem chemical transport model (v9-01-03) (Bey  
25 et al., 2001; Mao et al., 2013).

$$26 \quad \Omega_v = \Omega_s \frac{\int_0^{\infty} n(z) dz}{\int_0^{\infty} S(z) n(z) dz} \quad (1)$$

1 Here we use daily GEOS-Chem profiles spanning the observation period averaged between  
2 13:00-14:00 local time (LT), close to the satellite equatorial crossing time (13:38 LT). The  
3 satellite observations are gridded as seasonal averages on a  $0.5^\circ \times 0.5^\circ$  (lat x lon) grid. In this  
4 analysis, we use the averaged vertical column densities for June through August of 2007. The  
5 overlap between the satellite footprint and output grid is accounted for using an area-weighted  
6 tessellation algorithm (Liu et al., 2006). Satellite pixels with cloud fractions larger than 0.2  
7 (derived from the OMI O<sub>2</sub>-O<sub>2</sub> cloud algorithm (Stammes et al., 2008) and those impacted by the  
8 row anomaly (<http://www.knmi.nl/omi/research/product/rowanomaly-background.php>) are  
9 filtered before gridding.

10 The sources of errors in satellite measurements are numerous, including uncertainties in  
11 temperature-dependent absorption cross sections, the computation of the air mass factor,  
12 instrumental errors (e.g., wavelength calibration), potential interferences from other compounds,  
13 and low signal to noise. Seasonal averaging helps to reduce these errors. Assuming a 15%  
14 systematic uncertainty and following the formulation thoroughly explained in Vrekoussis et al.  
15 (2010), (section 4.3.1), the average error in satellite R<sub>GF</sub> over the SE US is 0.005, which is 18%  
16 of the average R<sub>GF</sub> value observed in this region.

17

### 18 **3 Results and Discussion**

19 Figure 1 shows daytime SENEX flight tracks colored by HCHO, CHOCHO, and R<sub>GF</sub>, with major  
20 emissions sources also indicated. Emissions information was acquired from the Continuous  
21 Emissions Monitoring Systems dataset for July - September of 2012  
22 (<http://ampd.epa.gov/ampd/>). In general, HCHO and CHOCHO mixing ratios are higher in the  
23 areas associated with high BVOC emissions (southern flights). In particular, high HCHO is  
24 observed over the Ozarks “isoprene volcano” (Wiedinmyer et al., 2005). The concentrations of  
25 both OVOCs are higher in regions with anthropogenic influence than in the surrounding  
26 biogenically dominated areas. Compared to the northern cities of Indianapolis and St. Louis,  
27 Birmingham and Atlanta have higher mixing ratios of HCHO and CHOCHO in their outflows.  
28 The Haynesville shale region has higher mixing ratios of both OVOCs, and CHOCHO is

1 especially enhanced. While HCHO and CHOCHO mixing ratios each vary by more than a factor  
2 of 4, the overall variability of  $R_{GF}$  observed during the SENEX flight campaign is low.

3 Boundary HCHO and CHOCHO measurements were also acquired during the Nashville/Middle  
4 Tennessee Ozone Study in June/July of 1995. While SENEX flight tracks more heavily sampled  
5 oil and natural gas fields, both studies are mainly representative of the isoprene-rich SE US. The  
6 average HCHO mixing ratio is similar (4.2 ppb in 1995, 4.4 ppb in this study), as is the average  
7 CHOCHO mixing ratio (0.07 ppb in 1995, 0.10 ppb in this study), leading to similar  $R_{GF}$  (1.7%  
8 in 1995, and 2.2% in this study) (Lee et al., 1998).

9 Figure 2 shows the same SENEX flight data gridded to the resolution of the OMI satellite  
10 retrievals ( $0.5^\circ \times 0.5^\circ$ ). Removing the flights with distinctly high or low  $R_{GF}$  observations (June  
11 10<sup>th</sup>, June 25<sup>th</sup>, and June 26<sup>th</sup>) the average gridded  $R_{GF}$  is  $2.5\% \pm 0.5\%$ , with a correlation  
12 coefficient between HCHO and CHOCHO of  $r^2 = 0.70$ . Below, we discuss these regions of  
13 notably high and low  $R_{GF}$  as well as the influence of urban emissions on the ratio.

14 Variability in the time of measurement may have an impact on the comparison of absolute  
15 concentrations of both OVOCs and  $R_{GF}$ , as measurements were acquired over a range of mid-day  
16 hours (~10:00-17:00 local time, see Table S1), and both HCHO and CHOCHO have strong  
17 diurnal cycles. By comparing the observations made within 1 hour on the same day, we aim to  
18 minimize any impact diurnal variation of  $R_{GF}$  would have on this analysis.

### 19 **3.1 Regions of high $R_{GF}$**

20 During flights on 10 June and 25 June, the region responsible for the high observed  $R_{GF}$  (4-7%)  
21 is in the southeast corner of the flight track, over the Kisatchie National Forest (Fig. 3a, 3b). The  
22 dominant tree species in this region is longleaf pine (<http://www.wlf.louisiana.gov>). Longleaf  
23 pine (*Pinus palustris*) is reported to emit monoterpenes but not isoprene (Rasmussen, 1972). The  
24 measured emission rate of  $\beta$ -pinene is the largest, and approximately 30% greater than the  $\alpha$ -  
25 pinene emission rate. All other monoterpenes emission rates are at least an order of magnitude  
26 lower (Geron et al., 2000). Indeed, measured monoterpene mixing ratios are elevated over this  
27 portion of the flight track (Fig. 3c, 3d), while isoprene (not shown) is relatively constant over the  
28 footprints of both flights. The high-monoterpene/high- $R_{GF}$  relationship is in agreement with the

1 Miller et al. (2014) satellite observation of high  $R_{GF}$  values above the boreal forests, where the  
2 high CHOCHO yield of monoterpenes is cited as the primary driver of  $R_{GF}$  (Fu et al., 2008). As  
3 in the two flights over the Kisatchie Forest, the June 26<sup>th</sup> flight also highlights a region with high  
4 monoterpenes and  $R_{GF} > 3\%$  (arrow on Fig. 4).

5 Also on the June 25<sup>th</sup> flight, high  $R_{GF} (> 8\%)$  is seen on the northeast side of the flight track  
6 (circled on Fig. 3b and 3d). Unlike the high  $R_{GF}$  associated with the monoterpenes emissions,  
7 these values are not replicated in the same area during the June 10<sup>th</sup> flight. In this region,  $R_{GF}$  is  
8 driven by a decrease in HCHO mixing ratio while the CHOCHO mixing ratio is slightly elevated  
9 (Fig. 5). Sharp features in meteorological measurements such as potential temperature, an  
10 increase in ozone, and a decrease in all other VOC and OVOC mixing ratios suggest an incursion  
11 of free tropospheric air. Given the lack of VOC precursors and other oxidation products, and  
12 assuming it is not a measurement artifact, the source of CHOCHO in the free troposphere is still  
13 unknown. The effect of trace gas vertical profile structure on the analysis of  $R_{GF}$  is examined in  
14 further detail in section 3.4.

### 15 **3.2 Regions of low $R_{GF}$**

16 On the June 26<sup>th</sup> flight, north of the gas production near the eastern side of the flight track,  
17 CHOCHO concentrations are low while HCHO mixing ratios are typical of other SENEX  
18 observations, driving  $R_{GF}$  to near 0% (Fig. 4). Concentrations of BVOC and AVOC precursors  
19 are also low in this region; however, methane mixing ratios are dramatically elevated. While  
20 isoprene is the dominant VOC in terms of calculated OH reactivity, increased HCHO relative to  
21 CHOCHO could be a result of oxidation of alkanes, which are associated with oil and natural gas  
22 (O&NG) production (Gilman et al., 2013). Gas flaring could also be a large source of direct  
23 HCHO emissions (Pikelnaya et al., 2013).

24 On the portion of the June 26<sup>th</sup> flight flown over the Mark Twain National Forest in the Missouri  
25 Ozarks (Fig. 4), the average  $R_{GF}$  is  $1.1 \pm 0.2\%$ . Here, the average isoprene concentration is high  
26 ( $7 \pm 2$  ppb), NO<sub>x</sub> is low ( $0.23 \pm 0.02$  ppb), and AVOC concentrations are low compared to  
27 BVOCs (toluene =  $0.06 \pm 0.01$  ppb). This suggests relatively pristine regions with strong  
28 isoprene emissions can be characterized by low  $R_{GF}$ . It is important to note that these  
29 measurements were acquired later in the day than most other measurements (~2:30 L.T, Table

1 S1), and approximately 3 hours later than the measurements acquired on the southwest portion of  
2 the flight track. We thus cannot rule out diurnal variation as an influence on  $R_{GF}$  in this region.

3 **3.3 Urban influence on  $R_{GF}$**

4 Because  $R_{GF}$  may be influenced by AVOC emissions and/or  $NO_x$  (Table 1), it has been proposed  
5 that  $R_{GF}$  can be used a diagnostic of the chemistry that leads to  $O_3$  formation (Vrekousiss et al.,  
6 2010; DiGangi et al., 2012; Li et al., 2014). Potential explanations for varying  $R_{GF}$  in urban areas  
7 include (1) preferential formation of one OVOC from AVOCs, (2) faster oxidation caused by  
8 high OH leading to different relative concentrations of the OVOCs, and (3) differing  $NO_x$   
9 dependencies of OVOC yields.

10 A comparison of in-plume and surrounding background measurements from the June 12<sup>th</sup> flight  
11 through Atlanta can help determine which of these factors may contribute to differences in  
12 observed  $R_{GF}$ . During this flight, northwesterly winds brought emissions from a nearby paper  
13 mill and power plant over the Atlanta area. As it travelled, the plume encountered emissions  
14 from the Atlanta international airport and other point and area sources. Figure 6 shows the flight  
15 path colored by CO, which demonstrates the boundary between background and polluted air.  
16 Figure 7 shows the mixing ratios of isoprene, toluene,  $NO_x$ , HCHO, CHOCHO, and the  
17 observed  $R_{GF}$  for the first four transects downwind of Atlanta.

18 Inside the plume,  $NO_x$  is enhanced, AVOCs such as toluene are high, BVOC mixing ratios are  
19 low, and concentrations of both OVOCs increased significantly (Fig 7). However, no clear  
20 distinction between in-plume and background measurements can be seen in  $R_{GF}$ . This trend in  
21 increasing HCHO and CHOCHO but consistent  $R_{GF}$  is also seen in several other flight tracks  
22 following urban outflow (for further examples, see Fig. S1 and S2 highlighting the July 5<sup>th</sup> flight  
23 over St. Louis).

24 There are two potentially compounding causes of the increase in HCHO and CHOCHO  
25 concentrations. First, direct emissions of the OVOCs or oxidation of AVOCs in the plume add to  
26 the background concentrations of HCHO and CHOCHO. While the oxidation of the observed  
27 AVOCs will increase OVOCs, the contribution of isoprene and its first generation oxidation  
28 products methyl-vinyl-ketone (MVK) and methacrolein (MACR) to OH reactivity is more than a

1 factor of 10 times greater than the contribution from measured AVOCs. Therefore, isoprene is  
2 still likely the dominant HCHO and CHOCHO precursor. Second, higher NO<sub>x</sub> in the plume  
3 leads to more efficient oxidation of VOCs, depleting mixing ratios of primary VOCs such as  
4 isoprene and increasing its oxidation products. This is consistent with the classical NO<sub>x</sub>-  
5 dependence of OH concentrations (Rohrer et al., 2014). The ratio of MVK and MACR to  
6 isoprene can be used as an indicator of the extent of photochemical processing (Fig. 7). The  
7 higher in-plume ratio of MVK+MACR to isoprene supports the conclusion that oxidation occurs  
8 faster in the plume. It is important to note that the low-NO<sub>x</sub> oxidation product ISOPOOH  
9 (isoprene hydroxy hydroperoxide) can interfere with PTR-MS measurements of MVK+MACR  
10 (Rivera-Rios et al., 2014), and potentially also measurements of HCHO. If ISOPOOH creates a  
11 positive bias MVK+MACR measurement, the artifact would be larger in the low-NO<sub>x</sub> areas,  
12 artificially increasing the (MVK+MACR)/isoprene ratio observed outside of the plume. Because  
13 (MVK+MACR)/isoprene is higher inside the plume, any interference would not affect the  
14 conclusion that oxidation occurs faster in the plume.

15 The absolute concentrations of HCHO and CHOCHO point to more rapid oxidation of isoprene  
16 in-plume as well as a potentially small contribution of AVOCs to both overall OVOC budgets,  
17 but neither of these characteristics influence  $R_{GF}$ . As stated above, a third potential driver of  $R_{GF}$   
18 is a difference in high- and low-NO<sub>x</sub> oxidation mechanisms. Again, though the NO<sub>x</sub>  
19 concentrations observed in-plume are significantly different than the surrounding air such that  
20 RO<sub>2</sub> spans different fates (reaction with NO versus reaction with HO<sub>2</sub> and isomerization), no  
21 characteristic change in  $R_{GF}$  is observed. Therefore,  $R_{GF}$  cannot be used to diagnose AVOC  
22 emissions, RO<sub>2</sub> fate, or OH levels in urban areas where isoprene emissions dominate the HCHO  
23 and CHOCHO budgets.

24 As discussed in section 3.2, the Ozarks demonstrated especially low  $R_{GF}$ . Both the Atlanta  
25 background air and the Ozarks are low-NO<sub>x</sub> isoprene-dominated regions (0.5 ppb NO<sub>x</sub> near  
26 Atlanta, 0.2 ppb NO<sub>x</sub> in the Ozarks), yet  $R_{GF}$  observations in these areas are significantly  
27 different. As previously discussed, urban emissions do not cause significant changes in  $R_{GF}$  if  
28 isoprene is the dominant VOC; therefore, some other factor must contribute to the comparably  
29 low  $R_{GF}$  over the Ozarks. While the observations of  $R_{GF}$  over the Ozarks were acquired at ~14:20  
30 L.T., later observations of  $R_{GF}$  in the plume background are not significantly different than the

1 earlier observations shown in Figure 7 ( $R_{GF}$  of  $2.2 \pm 0.3\%$  between 14:00 and 14:30 L.T.). This  
2 suggests that diurnal variation of  $R_{GF}$  is not the driving cause of the difference between Atlanta  
3 and Ozark observations.

4 The most notable difference between the regions is the observed concentrations of isoprene.  
5 Isoprene reached over 10 ppb in the Ozarks, while the Atlanta background air reached only 4  
6 ppb. A stronger relative contribution of monoterpenes to the HCHO and CHOCHO budgets in  
7 Atlanta could result in the higher observed  $R_{GF}$  (~50 ppt monoterpene/ppb isoprene near Atlanta,  
8 ~15 ppt monoterpenes/ppb isoprene near the Ozarks). Alternatively, the relationship of HCHO  
9 and CHOCHO with isoprene may be non-linear, with higher isoprene emissions leading to lower  
10  $R_{GF}$ . Because low- $NO_x$  isoprene oxidation is not well understood, especially with respect to OH  
11 concentrations (Rohrer et al., 2014), HCHO yields (Palmer et al., 2006; Marais et al., 2012), and  
12 CHOCHO yields (Stavrakou et al., 2009), model analysis cannot conclusively determine the  
13 cause of decreasing  $R_{GF}$  with increasing isoprene emissions. A model can be useful, however, in  
14 determining the anticipated influence of hydrocarbon speciation on  $R_{GF}$ , as discussed below.

### 15 **3.4 Modeled trends in $R_{GF}$ with hydrocarbon speciation**

16 The values of  $R_{GF}$  presented above suggest that (1) monoterpene oxidation leads to higher  $R_{GF}$   
17 than isoprene, (2) AVOCs must have substantially high concentrations to affect  $R_{GF}$  in regions  
18 with high isoprene emissions, and (3) depending on the surrounding BVOC emissions, alkanes  
19 could decrease the regional  $R_{GF}$ . To examine if these results are consistent with our  
20 understanding of the oxidation mechanisms of each VOC precursor, a simple 0-D box model  
21 analysis was performed using the University of Washington Chemical Box Model (UWCM)  
22 (Wolfe and Thornton, 2011), which incorporates the Master Chemical Mechanism v 3.2 (Jenkin  
23 et al., 1997; Saunders et al., 2003).

24 The intent of these model scenarios is not to compare modeled concentrations of CHOCHO and  
25 HCHO to their observed values, nor to compare modeled and measured  $R_{GF}$ , but to investigate  
26 the relative values of  $R_{GF}$  predicted by the model for each VOC precursor. Temperature, relative  
27 humidity,  $O_3$ , and CO are held at their observed campaign averages (297 K, 70%, 51 ppb, and  
28 140 ppb, respectively). OH is held at  $4 \times 10^6$  molec/cm<sup>3</sup>, and  $NO_x$  is constrained to the measured  
29 values representative of the plume background on 12 June (NO = 0.06 ppb;  $NO_2$  = 0.41 ppb).

1 The solar zenith angle is set to 13.4°, representative of the sun's position over Atlanta at 12:00  
2 local time on June 12<sup>th</sup>. Pressure is set to a constant 760 Torr, and all species are given an  
3 additional sink with a lifetime of 24 hours in lieu of explicitly modeling physical loss processes  
4 like deposition and dilution. The only hydrocarbon present in each model scenario is the VOC of  
5 interest, held at a constant concentration of 1 ppb. Integration time is set to 5 days, at which point  
6 the concentrations of both OVOCs are nearly constant. The calculated mixing ratios of  
7 CHOCHO and HCHO at the end of the model runs are shown in Table 2.

8 Compared to isoprene, the two monoterpenes investigated here ( $\alpha$ - and  $\beta$ -pinene) produce more  
9 CHOCHO per HCHO. As this effect has been demonstrated in model calculations, satellite  
10 observations, and flight-based measurements, we conclude that observations of high values of  
11  $R_{GF}$  are a result of high monoterpene compared to isoprene emissions. The absolute  
12 concentrations of both OVOCs produced from the oxidation of AVOCs studied here (benzene,  
13 toluene, ethene, ethyne, and the alkanes) are substantially lower compared to the yield from  
14 BVOCs. Because these AVOCs have long lifetimes, the concentration of AVOC would need to  
15 be substantially higher than BVOC to dominate the HCHO or CHOCHO budget. This is not  
16 likely in most of the SE US. However, AVOCs can dominate chemistry in O&NG production  
17 areas (Katzenstein et al., 2003; Edwards et al., 2014) and may be relatively more important in the  
18 winter when BVOC emissions are low or in areas with less vegetation. Alkanes and ethene  
19 produce less CHOCHO per HCHO compared to all BVOCs. In contrast, ethyne, benzene, and  
20 toluene produce much more CHOCHO relative to HCHO. The effect of AVOCs on  $R_{GF}$  is likely  
21 dependent on the speciation of emitted AVOCs, the strength of local BVOC emissions, and any  
22 direct OVOC emissions (e.g. HCHO from gas flaring). These compounding factors could make  
23 measurements of  $R_{GF}$  a convoluted diagnostic for assessing the VOC composition of different  
24 airmasses.

### 25 **3.5 Comparison with satellite retrievals**

26 While ideally 2013 OMI retrievals would be used in this analysis, the satellite has experienced  
27 severe degradation such that quantitative CHOCHO is not easily determined. Only the 2007  
28 retrievals are available at this time. One of the major conclusions reached using the SENEX in-  
29 situ measurements is that in the SE US,  $R_{GF}$  is not a diagnostic of anthropogenic emissions, as

1 HCHO and CHOCHO production are dominated by isoprene oxidation. Our in situ  
2 measurements also show that  $R_{GF}$  is unaffected by NO<sub>x</sub> and OH (Section 3.3). Therefore, as long  
3 as isoprene is the dominant VOC for HCHO and CHOCHO production in the SE US in both  
4 2007 and 2013, the comparison between 2007 satellite and 2013 in situ  $R_{GF}$  remains valid. Both  
5 this work and analysis of the previous 1995 Nashville/Middle Tennessee Ozone Study (Le et al.,  
6 1998) find isoprene to be the dominant HCHO source. Interannual variability of summertime  
7 isoprene emissions is estimated to be between 8 and 18% for the contiguous U.S. during the  
8 summers (Tawfik et al., 2012). Therefore, it is likely that isoprene is also the dominant OVOC  
9 source in 2007.

10 When comparing flight-based observations with satellite retrievals, it is important to consider the  
11 inherently different information these two measurements provide. Comparisons between column-  
12 integrated satellite retrievals and single-altitude measurements are only valid if the point  
13 measurements represent the seasonal mean of the behavior of the vertical column as a whole. To  
14 examine any effect of vertical distribution of HCHO and CHOCHO on satellite observations of  
15  $R_{GF}$ , we investigate the campaign average vertical profiles of both OVOCs, and  $R_{GF}$  calculated  
16 from those averages (Fig. 8). Both OVOCs show the expected decrease in concentration with  
17 altitude; however, the relative difference between boundary layer and free troposphere mixing  
18 ratios is greater for HCHO. This gives rise to a small increase in  $R_{GF}$  in the free troposphere. A  
19 higher free tropospheric  $R_{GF}$  was also observed in the 1995 Nashville/Middle Tennessee Ozone  
20 Study (Lee et al., 1998).

21 While  $R_{GF}$  is typically slightly higher in the free troposphere than the boundary layer, no clear  
22 altitude dependence in  $R_{GF}$  is observed within the boundary layer (Figure 8c, altitudes less than 2  
23 km, and figure S4 for individual profiles). In the free troposphere, CHOCHO measurements are  
24 below the detection limit (23 ppt at 3.25 km, detection limit = 32 ppt/5s). The observed  
25 variability in  $R_{GF}$  at high altitudes can largely be attributed to noise in the CHOCHO  
26 measurements at such low concentrations. Because the uncertainty in CHOCHO concentrations  
27 from measurement precision is typically greater than that from measurement accuracy, we take  
28 (Measured CHOCHO – 32 ppt) as the lower limit of CHOCHO as measured by ACES. If  
29 measurements are positively biased by as little as 16 ppt, which is within this range of  
30 uncertainty, corrected data would not demonstrate an increase in  $R_{GF}$  with altitude.

1 If the difference in HCHO and CHOCHO vertical structures is not a measurement artifact, the  
2 cause of the increase in  $R_{GF}$  in the free troposphere is unclear. VOC precursors with longer  
3 lifetimes that reach the free troposphere could preferentially form CHOCHO; however, all  
4 species of measured VOCs exhibit a similar steep decrease in concentration at high altitudes.  
5 Alternatively, the lifetimes of CHOCHO and HCHO could vary with altitude in such a way that  
6 HCHO concentrations show a more steep vertical dependence. However, this is unlikely as the  
7 photolysis and reaction with OH play nearly identical roles in the relative loss processes of the  
8 two OVOCs. Li et al. (2014) inferred different mixing layer heights for the two OVOCs. They  
9 calculated that the lifetime of isoprene was shorter than the typical boundary layer mixing time,  
10 and therefore hypothesized that HCHO production happened earlier (i.e. at lower altitudes) than  
11 CHOCHO production. In contrast, we see that the boundary layer is typically uniformly mixed  
12 with respect to HCHO and CHOCHO, potentially signifying the lifetime of the two OVOCs is  
13 longer than the boundary layer mixing time. Therefore, the time dependence of HCHO and  
14 CHOCHO production is unlikely to be the underlying cause of the difference in  $R_{GF}$  observed in  
15 the free troposphere. Finally, heterogeneous oxidation of aerosols has been proposed as a source  
16 of CHOCHO and other OVOCs in the free troposphere (Volkamer et al., 2015). No specific  
17 source of sufficient magnitude has been identified, but processes which release glyoxal, such as  
18 the ozonolysis of fatty acids (Zhou et al. 2014), would be potential candidates. Any such source  
19 would need to produce glyoxal in excess over formaldehyde.

20 Regardless of cause of the higher relative  $R_{GF}$  in the free troposphere, because the boundary  
21 layer contains the majority of HCHO and CHOCHO, the  $R_{GF}$  calculated from in situ HCHO and  
22 CHOCHO vertical column densities is only slightly higher than the average  $R_{GF}$  observed in the  
23 boundary layer (2.7% calculated from  $\Omega_V$ , 2.0% at 900 m). A similar analysis using each local  
24 vertical profile measurement rather than the campaign average vertical profiles yields the same  
25 conclusions. Table 3 lists the  $R_{GF}$  observed in the boundary layer and the  $R_{GF}$  calculated from in  
26 situ HCHO and CHOCHO vertical column densities for all profiles extending above 3 km, which  
27 were all flown in the Atlanta/Birmingham area. A map of profile locations, HCHO and  
28 CHOCHO measurements, and  $R_{GF}$  for each profile can be found in the supporting information  
29 (Fig. S3 and Fig. S4). In general, profiles with a smaller percentage of measurements acquired in  
30 the free troposphere do not display large difference between boundary layer and  $R_{GF}$  calculated

1 from in situ HCHO and CHOCHO vertical column densities. Individual profile measurements  
2 and campaign-averaged data support the conclusion that  $R_{GF}$  as observed by satellite retrievals  
3 should exhibit similar ranges as boundary layer observations, though a positive bias may be  
4 observed due to relatively higher CHOCHO in the free troposphere.

5 OMI satellite observations from June through August of 2007 over the United States are shown  
6 in Fig. 9. HCHO and CHOCHO are elevated over the SE US, where high isoprene emissions are  
7 expected to lead to increases in both OVOCs. Compared to the rest of the US,  $R_{GF}$  in this region  
8 is low. The northwest region of the US, where monoterpene emissions are high  
9 (Sakulyanontvittaya et al., 2008), demonstrates the highest  $R_{GF}$  over the US.

10 To compare satellite and flight-based observations, flight data were averaged to the  $0.5^{\circ} \times 0.5^{\circ}$   
11 OMI resolution. Summertime satellite retrievals and flight observations of CHOCHO v. HCHO  
12 show similar correlations, with  $r^2 \sim 0.4$ . (Fig. 10 and Table 4). The satellite average  $R_{GF}$  is  $\sim 0.6$   
13 percentage points higher than flight-based observations gridded to the same resolution. While  
14 this cannot be explained by the error and standard deviation of the gridded SENEX data and the  
15 uncertainty in the vertical column densities, this percentage is much smaller than the previous  
16 discrepancies between satellite and point-based measurements (DiGangi et al., 2012).

17 Figure 11 shows that while there is no correlation between satellite and flight  $R_{GF}$  ( $r^2 = 0.003$ ),  
18 the range of observed values are in good agreement (1.5-4%). Seasonal averages of  $R_{GF}$  from  
19 satellite retrievals are less likely to reflect extreme values and high-emission events compared to  
20 flight data, therefore high correlation is not anticipated at this time scale. Similarly, the  
21 correlation between satellite and ground HCHO ( $r^2=0.15$ ) and CHOCHO ( $r^2=0.044$ ) are low.  
22 Satellite and flight HCHO observations show stronger correlation than CHOCHO observations  
23 likely because CHOCHO aircraft measurements and satellite retrievals have higher relative  
24 uncertainties than HCHO retrievals (Miller et al., 2014; González Abad et al., 2105), and in situ  
25 CHOCHO measurements are close to the detection limit. The high and low values of  $R_{GF}$   
26 observed during the SENEX field campaign (June 25th and 26th flights) are not reproduced in  
27 the satellite observations A comparison of average BVOC emissions and O&NG production  
28 activity during the summer of 2007 and June 2013 would be needed to demonstrate that satellite  
29  $R_{GF}$  would be expected to show similar deviations from its average value. Furthermore, small

1 scale variation in satellite  $R_{GF}$  is mostly associated with noise, such that retrievals shown cannot  
2 distinguish the local influences (i.e. the Kisatchie National forest).

3 Besides the new CHOCHO retrieval method, one key distinction between this comparison and  
4 comparisons in previous studies (i.e., DiGangi et al., 2010) is the use of satellite retrievals for  
5 only the summer observational period rather the annual averages. Ground and flight based  
6 measurements are typically performed in the summer, when BVOC emissions are high.  
7 Therefore, point-based measurements may be biased to display the influence of BVOC emissions  
8 on  $R_{GF}$ .

9

#### 10 **4 Conclusions: Can $R_{GF}$ be used as a global indicator of VOC speciation?**

11 Overall, the flight-based measurements presented here show that  $R_{GF}$  is indicative of VOC  
12 speciation in select situations. High  $R_{GF}$  ( $>3\%$ ) is consistently observed in areas with high  
13 monoterpene emissions, and low  $R_{GF}$  ( $<2.5\%$ ) is associated with strong isoprene emissions. No  
14 consistent influence of AVOC or NO<sub>x</sub> emissions on the background  $R_{GF}$  was observed, likely  
15 because biogenic VOC emission strength determines  $R_{GF}$  in the SE US. The previously observed  
16 quick and short (2-5 min) increase in  $R_{GF}$  in DiGangi et al. (2010) may have been a result of  
17 extremely fresh emissions (e.g., diesel trucks emit at a rate of CHOCHO/HCHO = 9.4%  
18 (Schauer et al., 1999), and not indicative of larger scale changes in dominant VOC speciation.  
19 Emissions associated with oil and gas production areas can cause  $R_{GF}$  to deviate from the values  
20 observed over their background levels. However, the absolute value of  $R_{GF}$  in such regions is  
21 likely dependent on background BVOC emissions, speciation of AVOCs, and any direct OVOC  
22 emissions.

23 Compared to previous literature, absolute values of flight-based  $R_{GF}$  are in better agreement with  
24 satellite observations using the new CHOCHO retrieval algorithms. While time resolution plays  
25 a large role in direct comparisons of point-based measurements and satellite retrievals, the trend  
26 of high  $R_{GF}$  over areas with monoterpenes and low  $R_{GF}$  over areas with isoprene is broadly in  
27 agreement for the two platforms. With these trends validated by ground measurements,  $R_{GF}$   
28 based on satellite retrievals may be useful as a diagnostic of BVOC emissions. As these

1 retrievals become available at higher time and spatial resolution,  $R_{GF}$  can be used to help identify  
2 the speciation of VOCs leading to secondary pollutant formation on a regional scale.

3

4 **Acknowledgements**

5 The authors would like to acknowledge contribution from all members of the SENEX flight and  
6 science teams. Funding was provided by U.S. EPA-Science to Achieve Results (STAR)  
7 program- Grant 83540601. This research has not been subjected to any EPA review and  
8 therefore does not necessarily reflect the views of the Agency, and no official endorsement  
9 should be inferred. J. Kaiser acknowledges support from NASA Headquarters under the NASA  
10 Earth and Space Science Fellowship Program - Grant NNX14AK97H. This work was also  
11 supported as part of the NASA Aura Science Team.

12

13 **References**

14 Bey, I., Jacob, D. J., Yantosca, R. M., Logan, J. A., Field, B. D., Fiore, A. M., Li, Q. B., Liu, H.  
15 G. Y., Mickley, L. J., and Schultz, M. G.: Global modeling of tropospheric chemistry with  
16 assimilated meteorology: Model description and evaluation, *J. Geophys. Res.-Atmos.*, 106,  
17 23073-23095, 10.1029/2001jd000807, 2001.

18 Cazorla, M., Wolfe, G. M., Bailey, S. A., Swanson, A. K., Arkinson, H. L., and Hanisco, T. F.: A  
19 new airborne laser-induced fluorescence instrument for in situ detection of Formaldehyde  
20 throughout the troposphere and lower stratosphere, *Atmos. Meas. Tech. Discuss.*, 7, 8359-8391,  
21 10.5194/amt-7-8359-2014, 2014.

22 Christian, T. J., Kleiss, B., Yokelson, R. J., Holzinger, R., Crutzen, P. J., Hao, W. M., Saharjo, B.  
23 H., and Ward, D. E.: Comprehensive laboratory measurements of biomass-burning emissions. 1.  
24 Emissions from Indonesian, African, and other fuels, *J. Geophys. Res.*, 108, ACH3-1-13,  
25 10.1029/2002jd003704, 2003.

26 de Gouw, J., and Warneke, C.: Measurements of volatile organic compounds in the earths  
27 atmosphere using proton-transfer-reaction mass spectrometry, *Mass Spectrom. Rev.*, 26, 223-  
28 257, 10.1002/mas.20119, 2007.

1 DiGangi, J., Boyle, E., Karl, T., Harley, P., Turnipseed, A., Kim, S., Cantrell, C., Maudlin, R.,  
2 Zheng, W., Flocke, F., Hall, S., Ullmann, K., Nakashima, Y., Paul, J., Wolfe, G., Desai, A.,  
3 Kajii, Y., Guenther, A., and Keutsch, F.: First direct measurements of formaldehyde flux via  
4 eddy covariance: implications for missing in-canopy formaldehyde sources, *Atmos. Chem.  
5 Phys.*, 11, 10565-10578, 10.5194/acp-11-10565-2011, 2011.

6 DiGangi, J., Henry, S., Kamprath, A., Boyle, E., Kaser, L., Schnitzhofer, R., Graus, M.,  
7 Turnipseed, A., Park, J., Weber, R., Hornbrook, R., Cantrell, C., Maudlin, R., Kim, S.,  
8 Nakashima, Y., Wolfe, G., Kajii, Y., Apel, E., Goldstein, A., Guenther, A., Karl, T., Hansel, A.,  
9 and Keutsch, F.: Observations of glyoxal and formaldehyde as metrics for the anthropogenic  
10 impact on rural photochemistry, *Atmos. Chem. Phys.*, 12, 9529-9543, 10.5194/acp-12-9529-  
11 2012, 2012.

12 Edwards, P. M., Brown, S. S., Roberts, J. M., Ahmadov, R., Banta, R. M., deGouw, J. A., Dube,  
13 W. P., Field, R. A., Flynn, J. H., Gilman, J. B., Graus, M., Helmig, D., Koss, A., Langford, A.  
14 O., Lefer, B. L., Lerner, B. M., Li, R., Li, S.-M., McKeen, S. A., Murphy, S. M., Parrish, D. D.,  
15 Senff, C. J., Soltis, J., Stutz, J., Sweeney, C., Thompson, C. R., Trainer, M. K., Tsai, C., Veres,  
16 P. R., Washenfelder, R. A., Warneke, C., Wild, R. J., Young, C. J., Yuan, B., and Zamora, R.:  
17 High winter ozone pollution from carbonyl photolysis in an oil and gas basin, *Nature*, 514, 351-  
18 354, 10.1038/nature13767, 2014.

19 Fortems-Cheiney, A., Chevallier, F., Pison, I., Bousquet, P., Saunois, M., Szopa, S., Cressot, C.,  
20 Kurosu, T. P., Chance, K., and Fried, A.: The formaldehyde budget as seen by a global-scale  
21 multi-constraint and multi-species inversion system, *Atmos. Chem. Phys.*, 12, 6699-6721,  
22 10.5194/acp-12-6699-2012, 2012.

23 Fu, T.-M., Jacob, D. J., Wittrock, F., Burrows, J. P., Vrekoussis, M., and Henze, D. K.: Global  
24 budgets of atmospheric glyoxal and methylglyoxal, and implications for formation of secondary  
25 organic aerosols, *J. Geophys. Res.-Atmos.*, 113, 10.1029/2007jd009505, 2008.

26 Garcia, A. R., Volkamer, R., Molina, L. T., Molina, M. J., Samuelson, J., Mellqvist, J., Galle, B.,  
27 Herndon, S. C., and Kolb, C. E.: Separation of emitted and photochemical formaldehyde in  
28 Mexico City using a statistical analysis and a new pair of gas-phase tracers, *Atmos. Chem. Phys.*,  
29 6, 4545-4557, 2006.

1 Gilman, J. B., Lerner, B. M., Kuster, W. C., and de Gouw, J. A.: Source Signature of Volatile  
2 Organic Compounds from Oil and Natural Gas Operations in Northeastern Colorado, Environ.  
3 Sci. Technol., 47, 1297-1305, 10.1021/es304119a, 2013.

4 Goldstein, A. H., and Galbally, I. E.: Known and unexplored organic constituents in the earth's  
5 atmosphere, Environ. Sci. Technol., 41, 1514-1521, 10.1021/es072476p, 2007.

6 González Abad, G., Liu, X., Chance, K., Wang, H., Kurosu, T. P., and Suleiman, R.: Updated  
7 Smithsonian Astrophysical Observatory Ozone Monitoring Instrument (SAO OMI)  
8 formaldehyde retrieval, Atmos. Meas. Tech., 8, 19-32, 10.5194/amt-8-19-2015, 2015.

9 Greenberg, J. P., Friedli, H., Guenther, A. B., Hanson, D., Harley, P., and Karl, T.: Volatile  
10 organic emissions from the distillation and pyrolysis of vegetation, Atmos. Chem. Phys., 6, 81-  
11 91, 2006.

12 Guenther, A., Hewitt, C. N., Erickson, D., Fall, R., Geron, C., Graedel, T., Harley, P., Klinger,  
13 Lerdau, M., McKay, W. A., Pierce, T., Scholes, B., Steinbrecher, R., Tallamraju, R., Taylor,  
14 J., and Zimmerman, P.: A global model of natural volatile compound emissions, J. Geophys.  
15 Res.-Atmos, 100, 8873-8892, 10.1029/94jd02950, 1995.

16 Hays, M. D., Geron, C. D., Linna, K. J., Smith, N. D., and Schauer, J. J.: Speciation of gas-phase  
17 and fine particle emissions from burning of foliar fuels, Environ. Sci. Technol., 36, 2281-2295,  
18 10.1021/es0111683, 2002.

19 Holzinger, R., Warneke, C., Hansel, A., Jordan, A., Lindinger, W., Scharffe, D. H., Schade, G.,  
20 and Crutzen, P. J.: Biomass burning as a source of formaldehyde, acetaldehyde, methanol,  
21 acetone, acetonitrile, and hydrogen cyanide, Geophys. Res. Lett., 26, 1161-1164,  
22 10.1029/1999gl900156, 1999.

23 Hottle, J., Huisman, A., Digangi, J., Kamprath, A., Galloway, M., Coens, K., and Keutsch, F.: A  
24 Laser Induced Fluorescence-Based Instrument for In-Situ Measurements of Atmospheric  
25 Formaldehyde, Environ. Sci. Technol., 43, 790-795, 10.1021/es801621f, 2009.

26 Jenkin, M., Saunders, S., and Pilling, M.: The tropospheric degradation of volatile organic  
27 compounds: A protocol for mechanism development, Atmos. Environ., 31, 81-104,  
28 10.1016/S1352-2310(96)00105-7, 1997.

1 Kaiser, J., Li, X., Tillmann, R., Acir, I., Holland, F., Rohrer, F., Wegener, R., and Keutsch, F. N.:  
2 Intercomparison of Hantzsch and fiber-laser-induced-fluorescence formaldehyde measurements,  
3 *Atmos. Meas. Tech.*, 7, 1571-1580, 10.5194/amt-7-1571-2014, 2014.

4 Katzenstein, A. S., Doezena, L. A., Simpson, I. J., Balke, D. R., and Rowland, F. S.: Extensive  
5 regional atmospheric hydrocarbon pollution in the southwestern United States, *P. Natl. Acad.*  
6 *Sci. USA*, 100, 11975-11979, 10.1073/pnas.1635258100, 2003.

7 Kesselmeier, J., Bode, K., Hofmann, U., Muller, H., Schafer, L., Wolf, A., Ciccioli, P.,  
8 Brancaleoni, E., Cecinato, A., Frattoni, M., Foster, P., Ferrari, C., Jacob, V., Fugit, J. L., Dutaur,  
9 L., Simon, V., and Torres, L.: Emission of short chained organic acids, aldehydes and  
10 monoterpenes from *Quercus ilex* L. and *Pinus pinea* L. in relation to physiological activities,  
11 carbon budget and emission algorithms, *Atmos. Environ.*, 31, 119-133, 10.1016/s1352-  
12 2310(97)00079-4, 1997.

13 Lee, Y. N., Zhou, X., Kleinman, L. I., Nunnermacker, L. J., Springston, S. R., Daum, P. H.,  
14 Newman, L., Keigley, W. G., Holdren, M. W., Spicer, C. W., Young, V., Fu, B., Parrish, D. D.,  
15 Holloway, J., Williams, J., Roberts, J. M., Ryerson, T. B., and Fehsenfeld, F. C.: Atmospheric  
16 chemistry and distribution of formaldehyde and several multioxygenated carbonyl compounds  
17 during the 1995 Nashville Middle Tennessee Ozone Study, *J. Geophys. Res.*, 103, 22449-22462,  
18 10.1029/98JD01251, 1998.

19 Levelt, P. F., Van den Oord, G. H. J., Dobber, M. R., Malkki, A., Visser, H., de Vries, J.,  
20 Stammes, P., Lundell, J. O. V., and Saari, H.: The Ozone Monitoring Instrument, *IEEE Trans.*  
21 *Geosci. Remote Sens.*, 44, 1093-1101, 10.1109/tgrs.2006.872333, 2006.

22 Li, X., Rohrer, F., Brauers, T., Hofzumahaus, A., Lu, K., Shao, M., Zhang, Y. H., and Wahner,  
23 A.: Modeling of HCHO and CHOCHO at a semi-rural site in southern China during the PRIDE-  
24 PRD2006 campaign, *Atmos. Chem. Phys.*, 14, 12291-12305, 10.5194/acp-14-12291-2014, 2014.

25 Liu, X., Chance, K., Sioris, C. E., Kurosu, T. P., Spurr, R. J. D., Martin, R. V., Fu, T. M., Logan,  
26 J. A., Jacob, D. J., Palmer, P. I., Newchurch, M. J., Megretskaya, I. A., and Chatfield, R. B.: First  
27 directly retrieved global distribution of tropospheric column ozone from GOME: Comparison  
28 with the GEOS-CHEM model, *J. Geophys. Res.-Atmos.*, 111, 10.1029/2005jd006564, 2006.

1 MacDonald, S. M., Oetjen, H., Mahajan, A. S., Whalley, L. K., Edwards, P. M., Heard, D. E.,  
2 Jones, C. E., and Plane, J. M. C.: DOAS measurements of formaldehyde and glyoxal above a  
3 south-east Asian tropical rainforest, *Atmos. Chem. Phys.*, 12, 5949-5962, 10.5194/acp-12-5949-  
4 2012, 2012.

5 Mao, J., Paulot, F., Jacob, D. J., Cohen, R. C., Crounse, J. D., Wennberg, P. O., Keller, C. A.,  
6 Hudman, R. C., Barkley, M. P., and Horowitz, L. W.: Ozone and organic nitrates over the  
7 eastern United States: Sensitivity to isoprene chemistry, *J. Geophys. Res.-Atmos.*, 118, 11256-  
8 11268, 10.1002/jgrd.50817, 2013.

9 Marais, E. A., Jacob, D. J., Kurosu, T. P., Chance, K., Murphy, J. G., Reeves, C., Mills, G.,  
10 Casadio, S., Millet, D. B., Barkley, M. P., Paulot, F., and Mao, J.: Isoprene emissions in Africa  
11 inferred from OMI observations of formaldehyde columns, *Atmos. Chem. Phys.*, 12, 6219-6235,  
12 10.5194/acp-12-6219-2012, 2012.

13 McDonald, J. D., Zielinska, B., Fujita, E. M., Sagebiel, J. C., Chow, J. C., and Watson, J. G.:  
14 Fine particle and gaseous emission rates from residential wood combustion, *Environ. Sci.  
15 Technol.*, 34, 2080-2091, 10.1021/es9909632, 2000.

16 Miller, C. C., Abad, G. G., Wang, H., Liu, X., Kurosu, T., Jacob, D. J., and Chance, K.: Glyoxal  
17 retrieval from the Ozone Monitoring Instrument, *Atmos. Meas. Tech.*, 7, 3891-3907,  
18 10.5194/amt-7-3891-2014, 2014.

19 Palmer, P. I., Abbot, D. S., Fu, T.-M., Jacob, D. J., Chance, K., Kurosu, T. P., Guenther, A.,  
20 Wiedinmyer, C., Stanton, J. C., Pilling, M. J., Pressley, S. N., Lamb, B., and Sumner, A. L.:  
21 Quantifying the seasonal and interannual variability of North American isoprene emissions using  
22 satellite observations of the formaldehyde column, *J. Geophys. Res.-Atmos.*, 111,  
23 10.1029/2005jd006689, 2006.

24 Pikelnaya, O., Flynn, J. H., Tsai, C., and Stutz, J.: Imaging DOAS detection of primary  
25 formaldehyde and sulfur dioxide emissions from petrochemical flares, *J. Geophys. Res.-Atmos.*,  
26 118, 8716-8728, 10.1002/jgrd.50643, 2013.

1 Pollack, I. B., Lerner, B. M., and Ryerson, T. B.: Evaluation of ultraviolet light-emitting diodes  
2 for detection of atmospheric NO<sub>2</sub> by photolysis - chemiluminescence, *J. Atmos. Chem.*, 65, 111-  
3 125, 10.1007/s10874-011-9184-3, 2010.

4 Rasmusse, R. A.: What do the hydrocarbons from trees contribute to air pollution?, *J. Air Pollut.*  
5 *Contr. Assoc.*, 22, 537-543, 1972.

6 Rivera-Rios, J. C., Nguyen, T. B., Crounse, J. D., Jud, W., St. Clair, J. M., Mikoviny, T.,  
7 Gilman, J. B., Lerner, B. M., Kaiser, J. B., de Gouw, J., Wisthaler, A., Hansel, A., Wennberg, P.  
8 O., Seinfeld, J. H., and Keutsch, F. N.: Conversion of hydroperoxides to carbonyls in field and  
9 laboratory instrumentation: observational bias in diagnosing pristine versus anthropogenically-  
10 controlled atmospheric chemistry, *Geophys. Res. Lett.*, 2014GL061919,  
11 10.1002/2014GL061919, 2014.

12 Rohrer, F., Lu, K. D., Hofzumahaus, A., Bohn, B., Brauers, T., Chang, C. C., Fuchs, H., Haseler,  
13 R., Holland, F., Hu, M., Kita, K., Kondo, Y., Li, X., Lou, S. R., Oebel, A., Shao, M., Zeng, L.  
14 M., Zhu, T., Zhang, Y. H., and Wahner, A.: Maximum efficiency in the hydroxyl-radical-based  
15 self-cleansing of the troposphere, *Nature Geoscience*, 7, 559-563, 10.1038/ngeo2199, 2014.

16 Ryerson, T. B., Williams, E. J., and Fehsenfeld, F. C.: An efficient photolysis system for fast-  
17 response NO<sub>2</sub> measurements, *J. Geophys. Res.-Atmos.*, 105, 26447-26461,  
18 10.1029/2000jd900389, 2000.

19 Sakulyanontvittaya, T., Duhl, T., Wiedinmyer, C., Helmig, D., Matsunaga, S., Potosnak, M.,  
20 Milford, J., and Guenther, A.: Monoterpene and sesquiterpene emission estimates for the United  
21 States, *Environ. Sci. Technol.*, 42, 1623-1629, 10.1021/es702274e, 2008.

22 Saunders, S., Jenkin, M., Derwent, R., and Pilling, M.: Protocol for the development of the  
23 Master Chemical Mechanism, MCM v3 (Part A): tropospheric degradation of non-aromatic  
24 volatile organic compounds, *Atmos. Chem. Phys.*, 3, 161-180, 2003.

25 Schauer, J. J., Kleeman, M. J., Cass, G. R., and Simoneit, B. R. T.: Measurement of emissions  
26 from air pollution sources. 2. C-1 through C-30 organic compounds from medium duty diesel  
27 trucks, *Environ. Sci. Technol.*, 33, 1578-1587, 10.1021/es980081n, 1999.

1 Stammes, P., Sneep, M., De Haan, J. F., Veefkind, J. P., Wang, P., and Levelt, P. F.: Effective  
2 cloud fractions from the Ozone Monitoring Instrument: Theoretical framework and validation, *J.*  
3 *Geophys. Res.-Atmos.*, 113, 10.1029/2007jd008820, 2008.

4 Stavrakou, T., Muller, J.-F., De Smedt, I., Van Roozendael, M., Kanakidou, M., Vrekoussis, M.,  
5 Wittrock, F., Richter, A., and Burrows, J. P.: The continental source of glyoxal estimated by the  
6 synergistic use of spaceborne measurements and inverse modelling, *Atmos. Chem. Phys.*, 9,  
7 8431–8446, 10.5194/acp-9-8431-2009, 2009.

8 Tawfik, A. B., Stöckli, R., Goldstein, A., Pressley, S., and Steiner, A. L.: Quantifying the  
9 contribution of environmental factors to isoprene flux interannual variability, *Atmos. Environ.*,  
10 54, 216–224, 10.1016/j.atmosenv.2012.02.018, 2012.

11 Volkamer, R. et al., Aircraft measurements of bromine monoxide, iodine monoxide, and glyoxal  
12 profiles in the tropics: comparison with ship-based and in situ measurements, *Atmos. Meas.*  
13 *Tech. Discuss.*, 8, 623-687, 10.5194/amtd-8-623-2015, 2015.

14 Vrekoussis, M., Wittrock, F., Richter, A., and Burrows, J. P.: GOME-2 observations of  
15 oxygenated VOCs: what can we learn from the ratio glyoxal to formaldehyde on a global scale?,  
16 *Atmos. Chem. Phys.*, 10, 10145-10160, 10.5194/acp-10-10145-2010, 2010.

17 Washenfelder, R. A., Wagner, N. L., Dube, W. P., and Brown, S. S.: Measurement of  
18 Atmospheric Ozone by Cavity Ring-down Spectroscopy, *Environ. Sci. Technol.*, 45, 2938-2944,  
19 10.1021/es103340u, 2011.

20 Wiedinmyer, C., Greenberg, J., Guenther, A., Hopkins, B., Baker, K., Geron, C., Palmer, P. I.,  
21 Long, B. P., Turner, J. R., Petron, G., Harley, P., Pierce, T. E., Lamb, B., Westberg, H., Baugh,  
22 W., Koerber, M., and Janssen, M.: Ozarks Isoprene Experiment (OZIE): Measurements and  
23 modeling of the "isoprene volcano", *J. Geophys. Res.-Atmos.*, 110, 10.1029/2005jd005800, 2005.

24 Wolfe, G., and Thornton, J.: The Chemistry of Atmosphere-Forest Exchange (CAFE) Model -  
25 Part 1: Model description and characterization, *Atmos. Chem. Phys.*, 11, 77-101, 10.5194/acp-  
26 11-77-2011, 2011.

27 Zhou, S., Gonzalez, L., Leithead, A., Finewax, Z., Thalman, R., Vlasenko, A., Vagle, S., Miller,  
28 L. A., Li, S.-M., Bureekul, S., Furutani, H., Uematsu, M., Volkamer, R., and Abbatt, J.:

1 Formation of gas-phase carbonyls from heterogeneous oxidation of polyunsaturated fatty acids at  
2 the air-water interface and of the sea surface microlayer, *Atmos. Chem. Phys.*, 14, 1371-1384,  
3 10.5194/acp-14-1371-2014, 2014.

1 Table 1. Summary of previous published absolute values and trends of  $R_{GF}$ 

Reference	Method	$R_{GF}$ under biogenic influence (%)	$R_{GF}$ under anthropogenic influence (%)	Trend in $R_{GF}$ with anthropogenic influence
Vrekoussis et al. (2010)	Satellite	>4.5	<4.5	Decreasing
DiGangi et al. (2012)	LIF <sup>a</sup> /LIP <sup>b</sup> ; review of previous ground-based measurements	<2	>2.5	Increasing; independent of $NO_x$
MacDonald et al. (2012)	DOAS <sup>c</sup> ; model analysis	20-40	--	--
Li et al. (2014)	DOAS; model analysis	0.2-17		Generally increasing; depends on $NO_x$ , OH, and physical processes
Miller et al. (2014)	Satellite	<4 (isoprene) >4 (monoterpene)	~4	Depends on BVOC
This work	LIF/ACES <sup>d</sup>	<2.5 (isoprene) >3 (monoterpene)	variable	Depends on BVOC and AVOC

2 <sup>a</sup>Laser Induced Fluorescence (HCHO)3 <sup>b</sup>Laser Induced Phosphorescence (CHOCHO)4 <sup>c</sup>Differential Optical Absorption Spectroscopy5 <sup>d</sup>Airborne Cavity Enhanced Spectrometer (CHOCHO)

1 Table 2. Relative abundance of HCHO and CHOCHO from 1 ppb of a given precursor<sup>a</sup>

Precursor	CHOCHO	HCHO	Ratio (%) <sup>b</sup>
Isoprene	0.27 ppb	4.3 ppb	6.3
$\alpha$ -pinene	0.31 ppb	3.6 ppb	8.6
$\beta$ -pinene	0.49 ppb	3.6 ppb	14
Ethane	0.02 ppt	5.4 ppt	0.4
Ethene	586 ppt	24 ppt	4.2
Ethyne	0.91 ppt	14 ppt	1500
Propane	0.02 ppt	8.8 ppt	0.2
n-butane	1.5 ppt	140 ppt	1.1
Benzene	23 ppt	7.6 ppt	303
Toluene	103 ppt	150 ppt	69

2 <sup>a</sup>Calculated using a 0-D box model. See text for details.

3 <sup>b</sup>Ratio = CHOCHO/HCHO

1 Table 3. Comparison of column-integrated and boundary layer  $R_{GF}$

Profile number	Boundary layer $R_{GF}$ <sup>a</sup>	$R_{GF}$ calculated from in situ HCHO $\Omega_V$ and CHOCHO $\Omega_V$	Difference <sup>b</sup>	% of altitude range in FT <sup>c</sup>
1	2.7	3.2	0.6	68
2	2.2	2.6	0.4	53
3	2.7	3.4	0.7	50
4	2.0	2.1	0.1	50
5	1.7	2.1	0.4	50
6	1.9	2.2	0.3	47
7	2.4	2.2	-0.2	42
8	1.9	1.9	0.0	17
9	2.1	2.1	0.0	15
10	2.5	1.9	-0.7	15
11	2.6	2.4	-0.2	8
12	2.0	2.1	0.1	8

2 <sup>a</sup>Observed at 1 km

3 <sup>b</sup>Calculated as column-integrated  $R_{GF}$  - boundary layer  $R_{GF}$

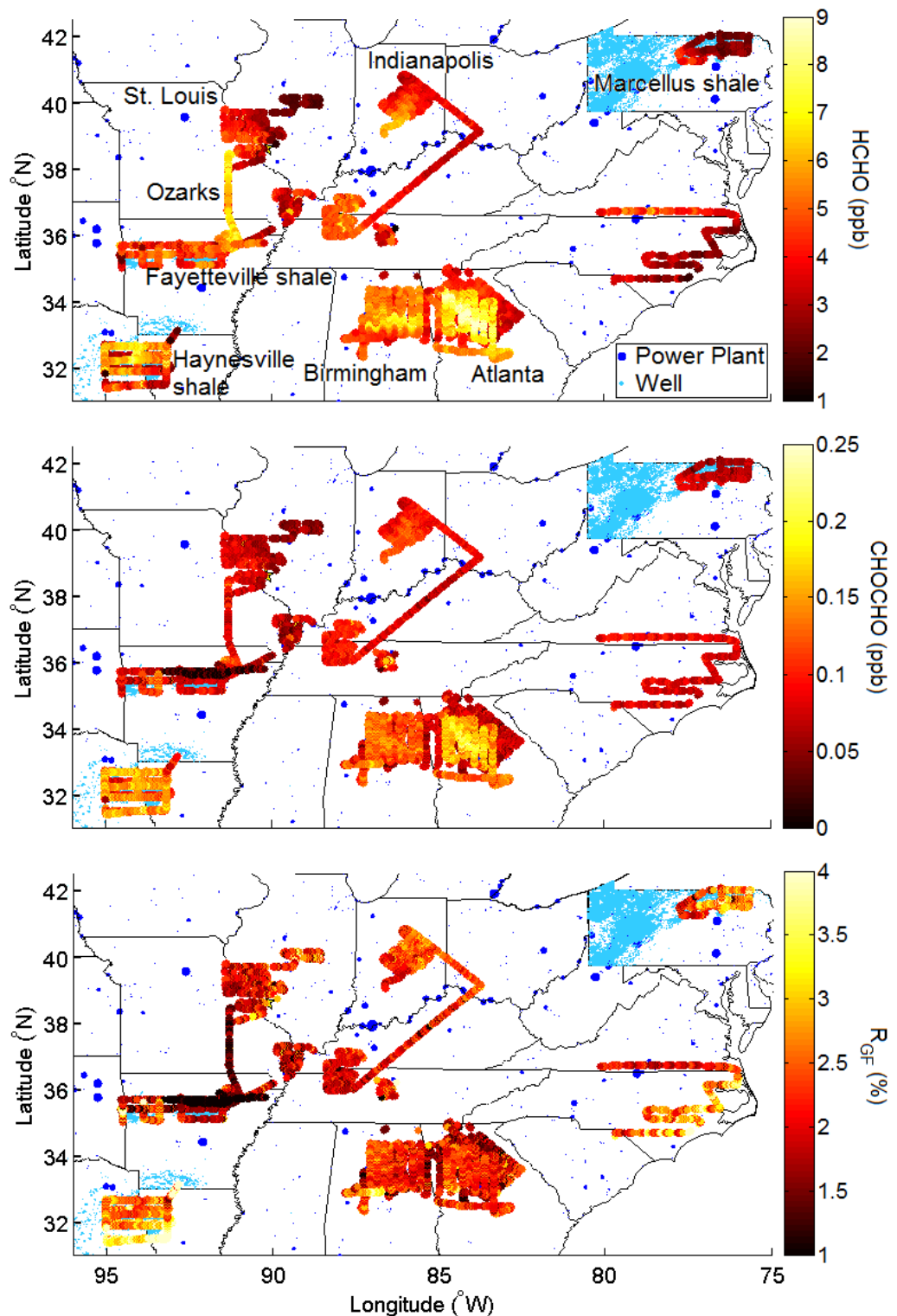
4 <sup>c</sup>FT = Free troposphere. Boundary layer height determined by gradient in  $O_3$

1 Table 4. Linear fits of CHOCHO v. HCHO observations<sup>a</sup>

Method	Slope	Intercept	$r^2$	Average $R_{GF}$ (%)
Flight	0.017	0.019 ppb	0.43	2.2
Satellite	0.024	$\sim 0.016$ ppb <sup>b</sup> $(6.6 \times 10^{13} \text{ molec/cm}^2)$	0.38	2.8

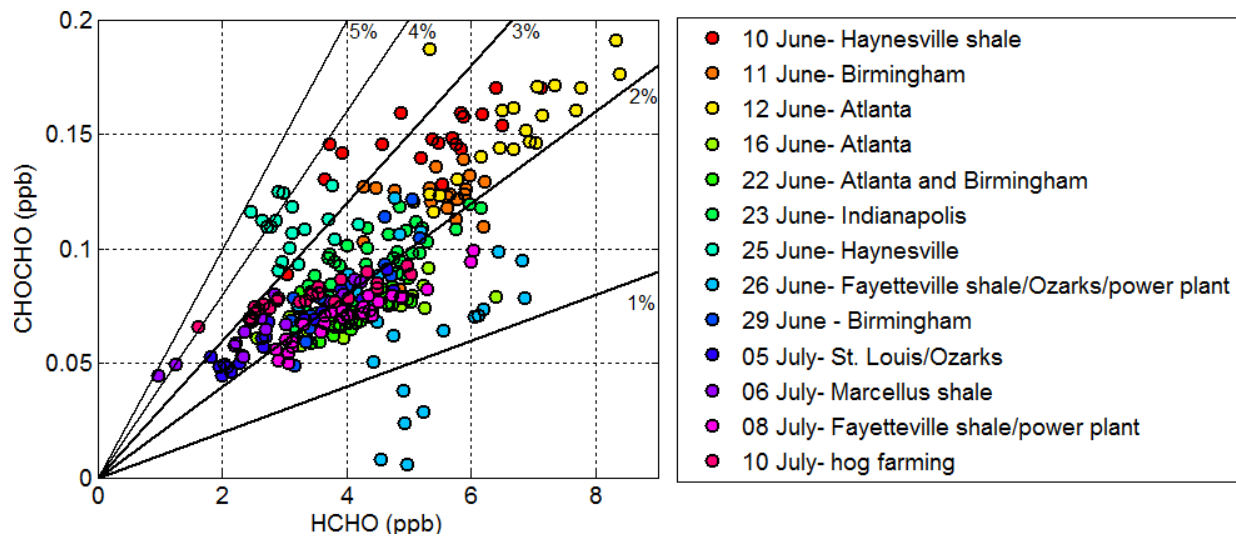
2 <sup>a</sup>All data are gridded to  $0.5^\circ \times 0.5^\circ$  resolution for orthogonal distance regression analysis. For  
 3 SENEX flight observations, all flights (including Haynesville and Fayetteville areas) are  
 4 included.

5 <sup>b</sup>Ground level mixing ratio was calculated assuming CHOCHO and HCHO are contained within  
 6 a well mixed 1500 m boundary layer and an atmospheric scale height of 7.5 km.



1

2 Figure 1. Daytime flight tracks colored by HCHO, CHOCHO, and  $R_{GF}$ . Power plant markers are  
3 scaled by  $\text{NO}_x$  emissions.



1 Figure 2. The relationship of CHOCHO and HCHO for each flight, gridded to OMI satellite  
 2 resolution. Flights with extreme values of  $R_{GF}$  include those to the Haynesville shale (10 June  
 3 and 25 June) and the Ozarks (26 June).  
 4

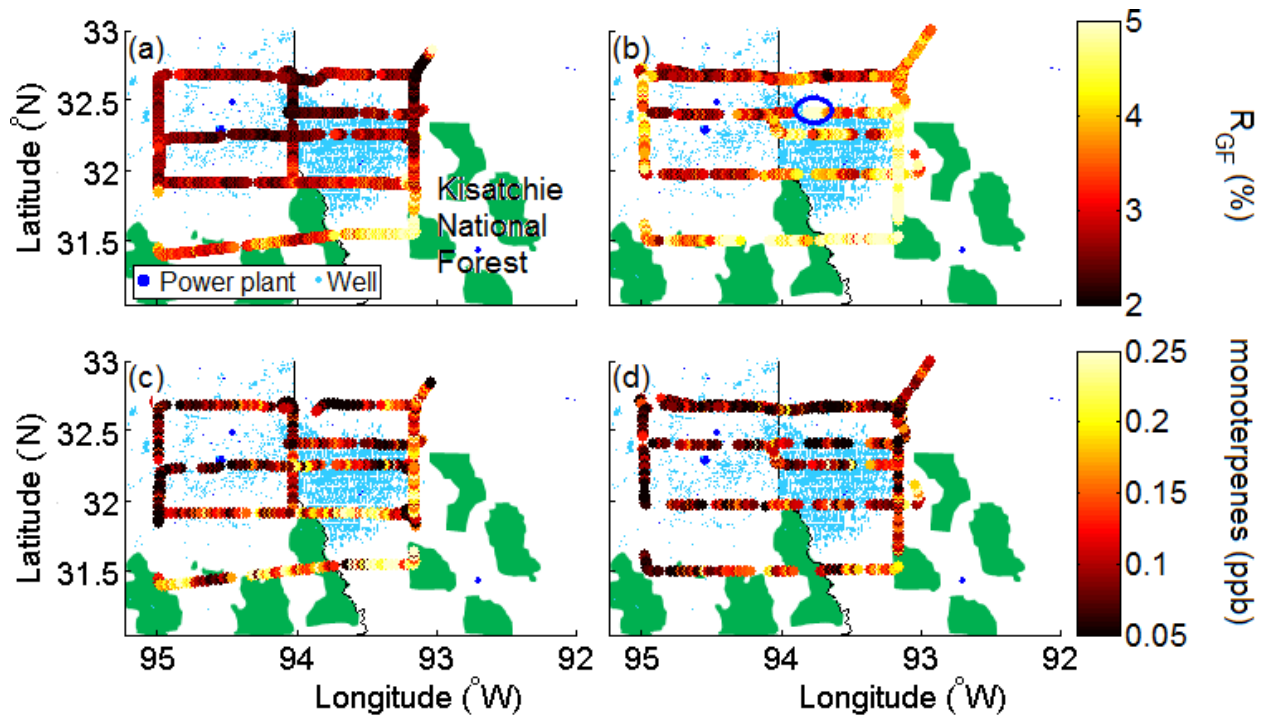
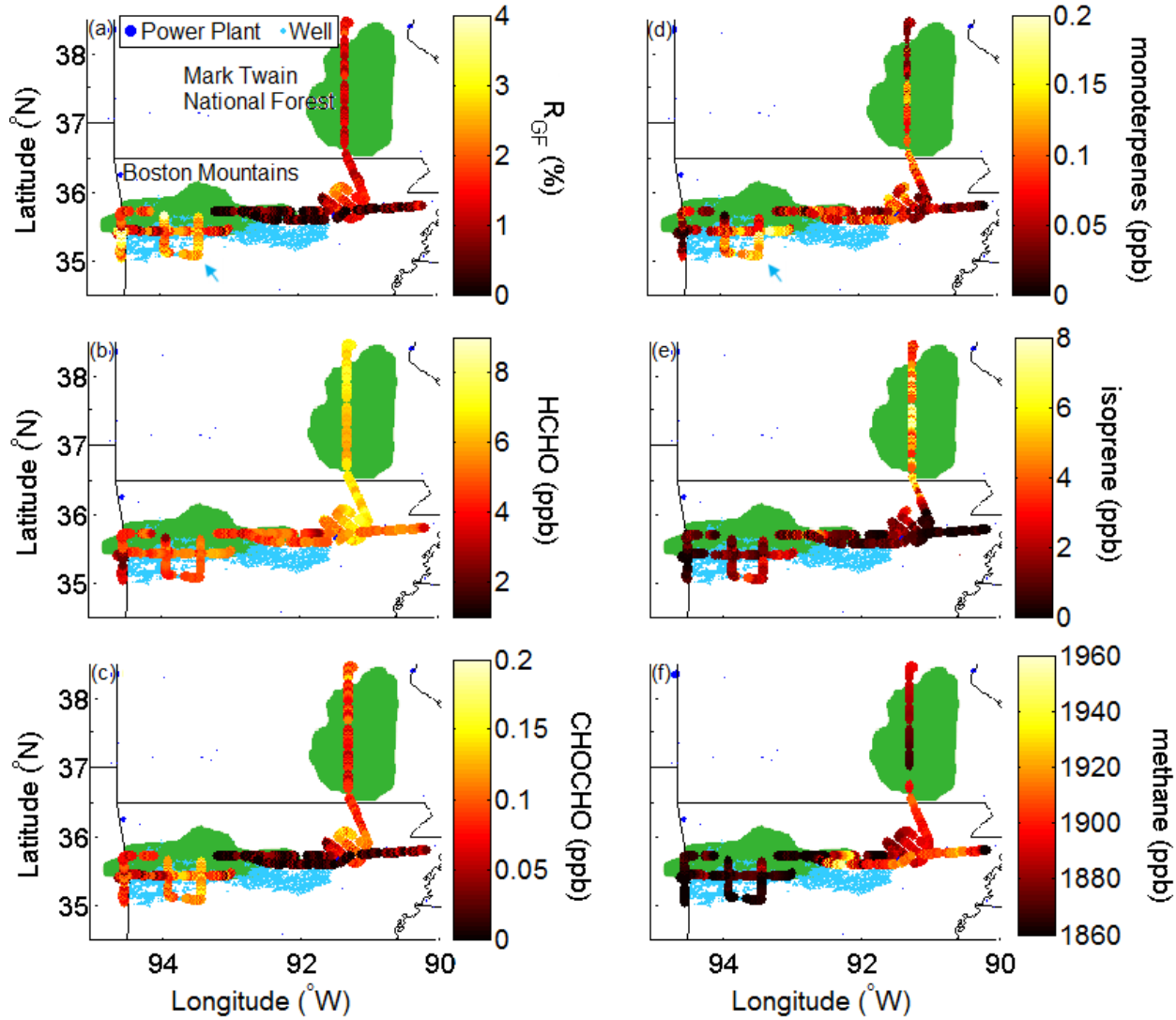
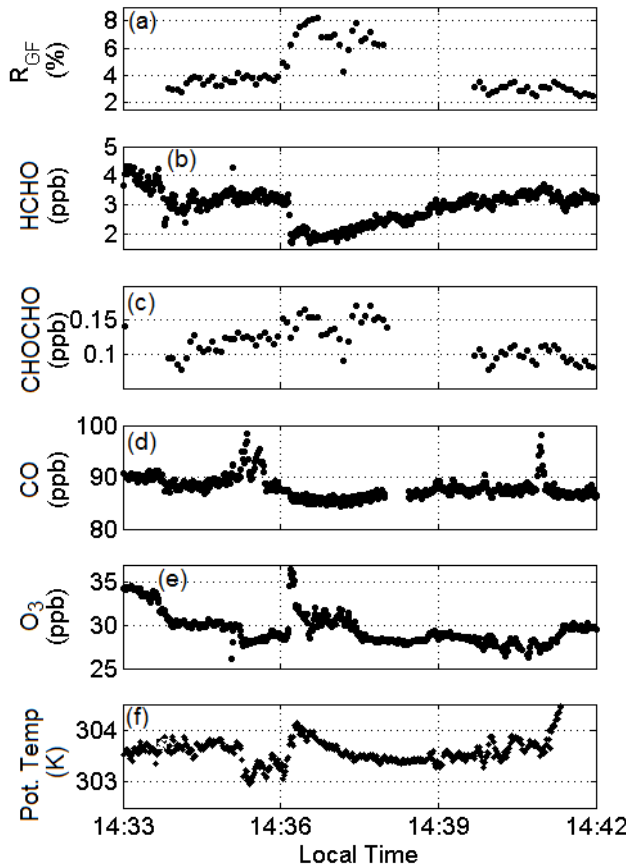


Figure 3. Flight tracks for 10 June (a, c) 25 June (b,d) over the Haynesville shale, colored by  $R_{GF}$  and the measured monoterpene mixing ratio. The southeast corner highlights high  $R_{GF}$  in a region with high monoterpene concentrations. The blue circle indicates the location of high  $R_{GF}$  discussed further in the text. Figure 5 shows meteorological and trace gas measurements acquired at this location. National parks are shown in green, and the Kisatchie National Forest is labeled in (a).

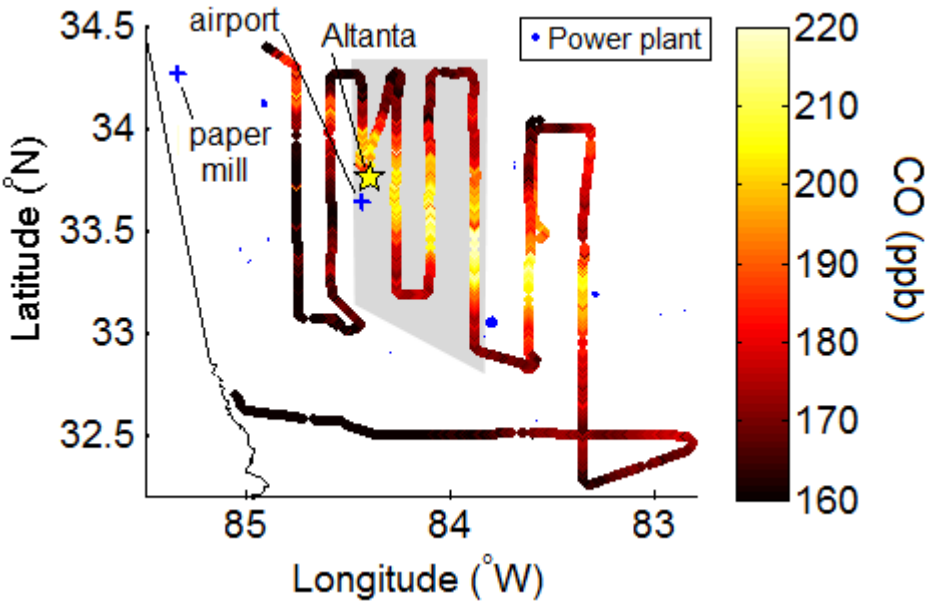


1

2 Figure 4. Flight track for the 26 June over the Fayetteville shale, the independence power plant,  
3 and the Ozarks, colored by the specified trace gas mixing ratio and  $R_{GF}$ . The blue arrow  
4 highlights the region of elevated monoterpenes. National forests are shown in green.



1  
2 Figure 5. Time series of specified measurements during the rapid increase in  $R_{GF}$  observed south  
3 of Shreveport on the 25 June flight (blue circle in Fig. 3). An incursion of free tropospheric air  
4 near 14:36 L.T. drives high  $R_{GF}$ .



1  
2 Figure 6. Flight track for 12 June colored by CO, which shows the combined outflow of Atlanta,  
3 the airport, and a paper mill on the surrounding background. Measurements acquired in the  
4 shaded area are shown in Fig. 7.

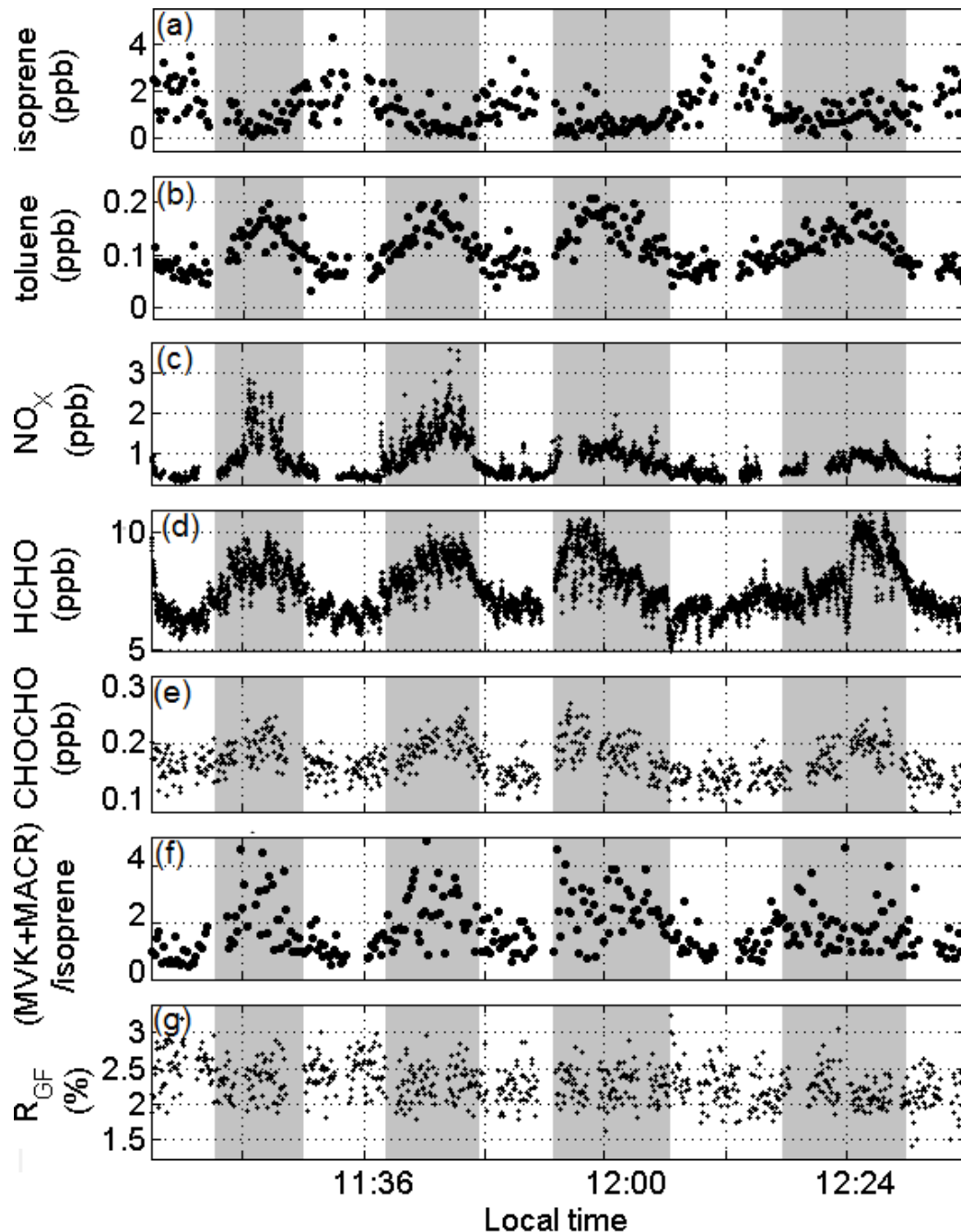
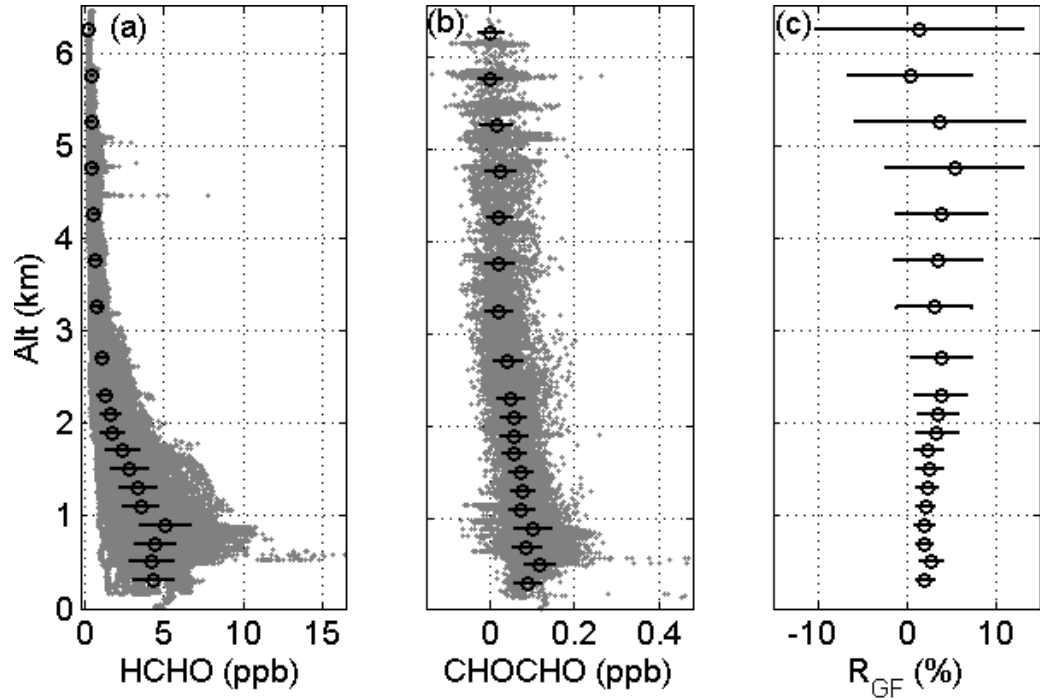
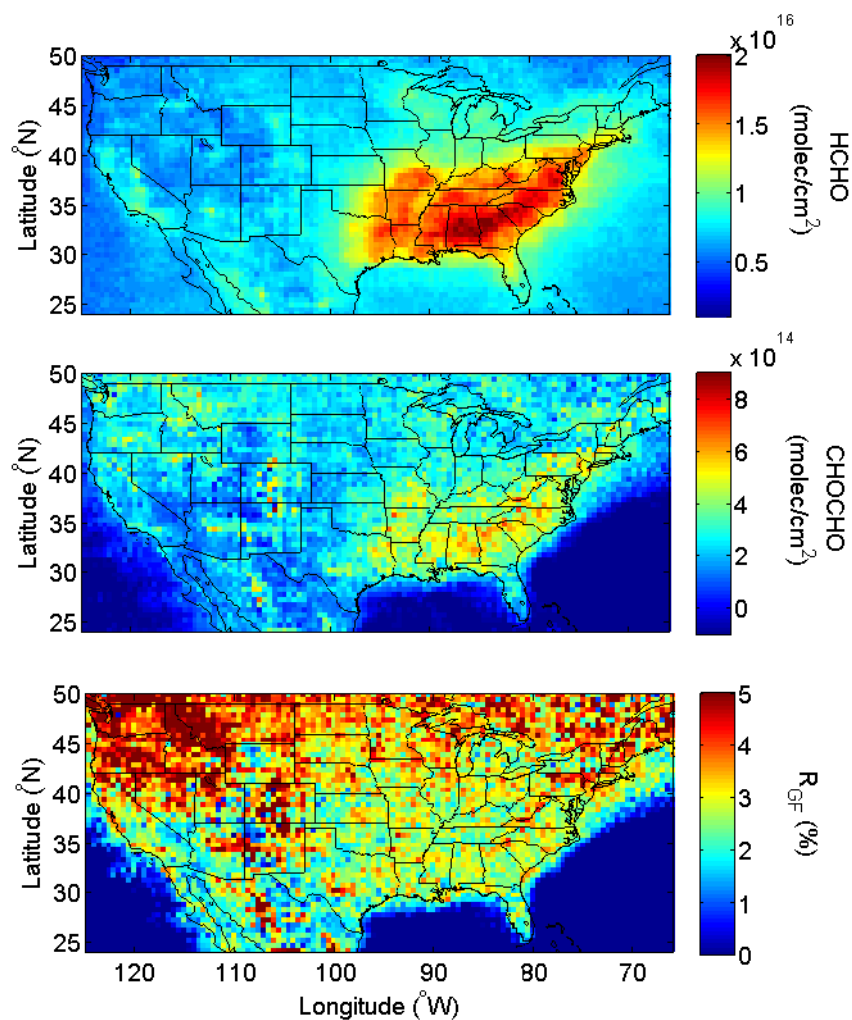


Figure 7. Measurements acquired on the 12 June flight corresponding to the boxed in region in Fig. 6. Shaded regions indicate high anthropogenic influence. While the measurements alter between AVOC/high NO<sub>x</sub> and BVOC/low NO<sub>x</sub> regimes, little change is seen in R<sub>GF</sub>. The maximum values of NO<sub>x</sub> and (MVK+MACR)/isoprene fall above the limits shown here.

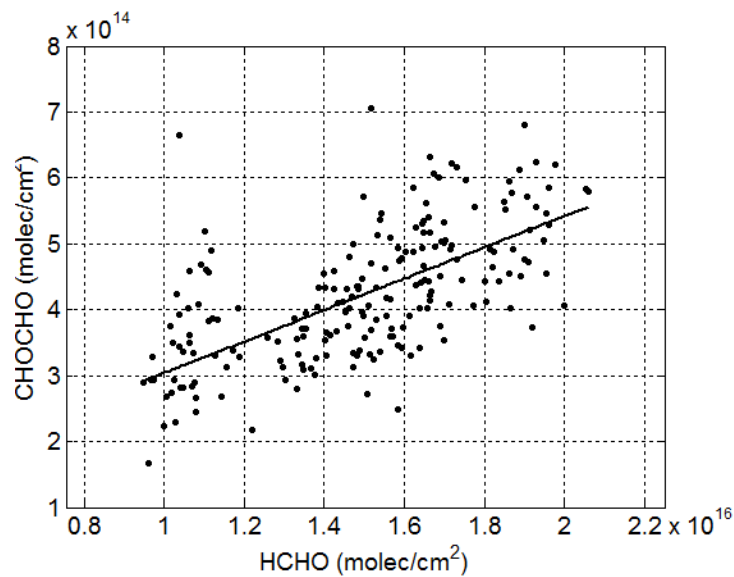


1 Figure 8. Average vertical profile of (a) HCHO and (b) CHOCHO measurements acquired  
 2 during the flights specified in Fig. 1. Gray dots represent all measurements, black circles are  
 3 averages in a given altitude bin, and error bars are standard deviation within that bin. Bins are  
 4 200 m in height from 200 to 2500 m, and 500 m thereafter. (c)  $R_{GF}$  calculated from average  
 5 HCHO and CHOCHO profiles. Error bars are calculated from the standard deviations of HCHO  
 6 and CHOCHO observations.

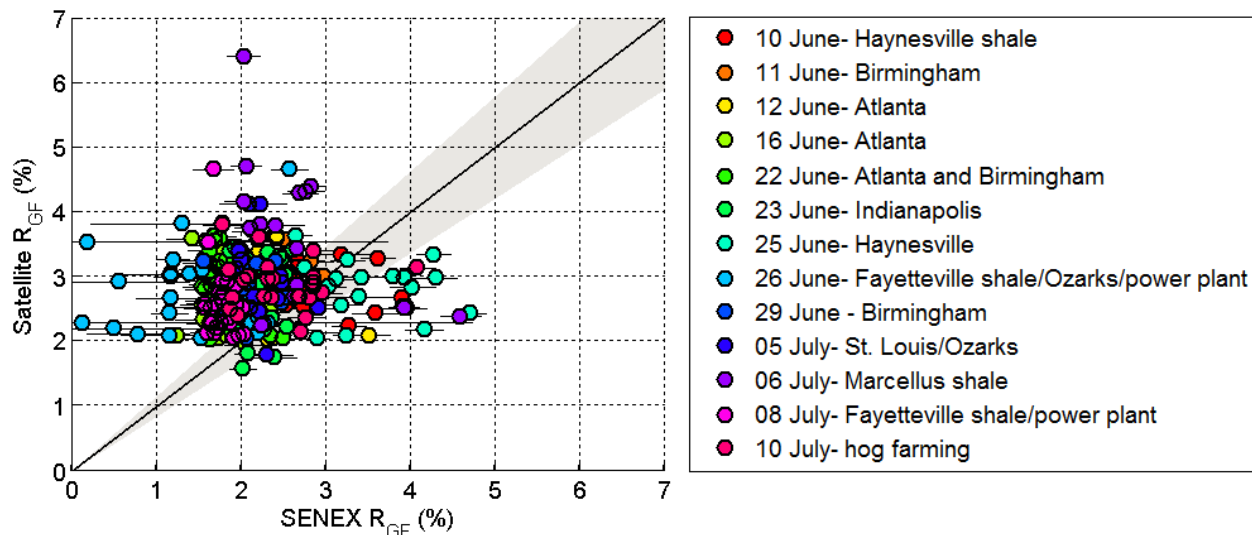


1

2 Figure 9. OMI Satellite retrievals of HCHO and CHOCHO vertical density during June through  
 3 August of 2007. The ratio to CHOCHO to HCHO is shown in the bottom panel.



1      Figure 10. Satellite retrieval of CHOCHO v HCHO corresponding to grid coordinates of SENEX  
2      boundary layer measurements. Statistics for the linear fits are shown in Table 4.  
3



1

2 Figure 11. Satellite and SENEX  $R_{GF}$ . The line represents a 1-1 relationship, error bars represent  
 3 standard deviations of SENEX measurements within the given pixel, and the shaded area  
 4 represents the accuracy of the SENEX measurements.